AMD-Vol. 217, Rheology and Fluid Mechanics of Nonlinear Materials
ASME 1996

THE MOTION AND INTERACTION OF SOLID PARTICLES IN VISCOELASTIC LIQUIDS

J. Feng
Department of Chemical Engineering,
University of California, Santa Barbara, California 93106

D. D. Joseph and P. Y. Huang
Department of Aerospace Engineering and Mechanics,
University of Minnesota, Minneapolis, Minnesota 55455

ABSTRACT

In this paper we present numerical and experimental results on the motion and interaction of solid particles in polymeric fluids. The two-dimensional numerical work investigates the viscoelastic effects on the sedimentation of a particle in the presence of solid walls or another particle. The Navier-Stokes equations coupled with an Oldroyd-B model are solved using a finite element method, and the particles are moved according to their equations of motion. In a vertical channel, a particle settling close to one side wall experiences a repulsion from the wall; a particle settling farther away from the wall is attracted to it. Two particles settling in tandem attract and form a doublet if their initial separation is not too large. Two particles settling side by side approach each other and the doublet also rotate till the line of centers is aligned with the direction of fall. The experimental part studies the behavior of single particles and suspensions in polymer solutions in a torsional flow. Four issues are investigated: the radial migration of a spherical particle, the rotation and migration of a cylindrical rod, the particle-particle interaction and microstructures in a suspension of spheres and the microstructures in a suspension of rods. A spherical particle migrates outward at a constant velocity unless the polymer solution is very dilute. A rod has two modes of motion depending on its shape, initial orientation, the local shear rate and the magnitude of normal stresses in the fluid. When a suspension is sheared, spheres form chains along the flow direction. These chains may connect and form circular rings, which migrate outward at a velocity much higher than that for a single sphere. Rods interact with each other and aggregate in much the same way, but to a less extent than spheres. Particle interaction and aggregation can be explained by two fundamental mechanisms discovered in the numerical simulations of sedimentation.

1. Introduction

Solid particles are added to polymer melts to lower cost or to achieve desirable properties. In processing such composite materials, it has been observed that the solids tend to migrate across streamlines and form aggregates, and fibers exhibit complex orientation depending on the flow field. Thus, inhomogeneity and anisotropy occur in the finished product. Experiments on these phenomena tend to be qualitative and the explanations offered are usually speculative (e.g., Toll & Andersson 1993). The main reason is that most of these studies strive to approximate the complex geometry and flow fields in polymer processing. Direct tracking of individual particles under these experimental conditions is impossible, thus rendering arguments on particle behavior tentative.

Much research effort has been expended on modeling the flow of solid-filled polymers. Unfortunately, all models up to now fall far short of accounting for the solid behavior mentioned above. Solid fibers are assumed to follow the Jeffery orbit, which applies rigorously only to creeping flows of Newtonian fluids. Fiber-fiber interaction is modeled as a Brownian-like diffusion (Advani & Tucker 1987). Ait-Kadi & Grmela (1994) is the only work that allows for viscoelastic media: the extra stress of the fluid is given by a FENE-P model and the solid contribution to the stress is given by the Dinh-Armstrong equation (Dinh & Armstrong 1984) modified to include non-Newtonian effects on the drag. This is the most sophisticated model that we have seen. Yet by no means can fiber aggregation and migration be simulated because the non-linear mechanisms for these scenarios are not understood.

Therefore, a wide gap exists between the complexity of flows under realistic processing conditions and the capability of continuum modeling. This points to the need for studying the local mechanisms of particle migration and interaction. Previous work has identified viscoelastic normal stresses and inertia as the nonlinear mechanisms for the intriguing behavior of particles (Leal 1980). Interestingly, the two nonlinearities almost always oppose each other in their effects on particle motions. Here we are mainly concerned with the normal stress effects.

Three features of particle motion have received special attention: the lateral migration of spheres, the orientation or rotation of long particles and the interactions between particles. These have been observed in sedimentation and various forms of shear flows. An elongated particle settling in a quiescent liquid rotates till its long axis aligns with the fall (Leal 1975, Liu & Joseph 1993). A rod-like particle in a shear flow approaches a limiting orbit of rotation with its axis aligned with the vorticity vector (Karnis & Mason 1966, Gauthier *et al.* 1971*ab*). If the fluid has strong normal stresses and the shear rate is

sufficiently high, the rod may align itself with the streamline (Bartram *et al.* 1975). In a Poiseuille flow, a particle migrates across streamlines to the center of the pipe (Gauthier *et al.* 1971*b*, Karnis & Mason 1966). Two spheres sedimenting one above another may attract or repel depending on their initial separations (Riddle *et al.* 1977). Spheres form structures that are aligned with the stream in shear flows (Highgate & Whorlow 1968, Giesekus 1981). More recently, Prieve and co-workers studied the radial migration of a sphere in a torsional shear flow between parallel disks. A solid sphere migrates inward in a 1% polyisobutylene in polybutene solution (Karis *et al.* 1984*a*). Later experiments using more dilute solutions discovered that the sphere migrates inward if the initial position is within a critical radius and migrates outward otherwise (Karis *et al.* 1984*b*, Prieve *et al.* 1985, Choi *et al.* 1987). Joseph *et al.* (1994) studied the effects of a nearby wall on a sedimenting sphere and the interaction between two spheres settling side by side. In a Newtonian fluid, inertia is known to cause repulsion between the sphere and the wall and between the two spheres (Liu *et al.* 1993). In viscoelastic liquids, the sphere is pulled toward the wall and the two spheres attract if the initial separation is smaller than a critical value, beyond which no interaction is discernible.

Perturbation theories based on the second-order fluid model have achieved remarkable success in predicting the motion of particles (Leal 1979, Brunn 1980). Qualitatively correct predictions have been obtained for the preferred orientation of a settling long body (Leal 1975), the lateral migration of a sphere in a non-homogeneous shear flow (Ho & Leal 1976, Chan & Leal 1977) and the evolution of the Jeffery orbit (Leal 1975). However, when Brunn (1977) applied the same scheme to the interaction of two sedimenting spheres, results show that the two spheres always attract, in apparent disagreement with the observations of Riddle *et al.* (1977). Caswell (1972) used a similar perturbation procedure to study the wall effects on the sedimentation of a sphere. His results show that the sphere would be repelled by the wall, again in contradiction to experimental observations. In a torsional shear, the theory predicts an inward migration of particles, which is in apparent agreement with the observations of Karis *et al.* (1984*a*). But the theory fails to explain the two-way migration later observed in more dilute solutions.

In this paper, we present numerical simulations of wall-particle and particle-particle interactions in sedimentation and experimental observations of the behavior of single particles and suspensions in torsional shear. The numerical work was inspired by the failure of perturbation theories mentioned above. The Navier-Stokes equations coupled with an Oldroyd-B model are solved using a finite element method, and the particles are moved according to their equations of motion. The nonlinear inertia and normal stresses are fully taken into account. Two problems are studied in this paper: the sedimentation of a circular particle released in a vertical channel at various initial distances from one side wall and the sedimentation of a pair of particles released side by side or in tandem. Because the Newtonian counterparts of these problems have been studied (Feng *et al.* 1994*a*, Liu *et al.* 1993), the effects of normal stresses can be highlighted. The experimental effort was inspired by the work of Prieve *et al.* (1985). We will investigate the radial migration of spheres using a different kind of polymer solution. The behavior of rods and suspensions of spheres and rods are also studied. Microstructures in suspensions of spheres have been previously reported (Giesekus 1981), but ours appears to be the first well-controlled experiment in a steady non-homogeneous shear flow. The formation of microstructures in sheared suspensions provides direct testimony to the nonlinear mechanisms discovered in numerical analyses.

2. Numerical results and discussions

Our algorithm is an extension of what was used in simulating moving boundary problems in Newtonian fluids (Feng *et al.* 1994*ab*). The equations of motion and the constitutive equation are:

$$\nabla \cdot \mathbf{u} = 0$$

$$\rho_f \left(\frac{\partial \mathbf{u}}{\partial t} + \mathbf{u} \cdot \nabla \mathbf{u} \right) = -\nabla p + \nabla \cdot \mathbf{T}$$

$$\mathbf{T} + \lambda_1 \overset{\nabla}{\mathbf{T}} = 2\mu \left(\mathbf{D} + \lambda_2 \overset{\nabla}{\mathbf{D}} \right)$$

At each time step, the above equations are solved using a finite element solver POLYFLOW with an EVSS scheme. The force and torque on the solid particle then determine the position and velocity of the particle at the next time step. The new domain is re-meshed and the old velocity and stress fields are projected onto the new mesh. Then the velocity, pressure, stress and deformation gradient fields are computed for the new time. More details of the algorithm and the mesh are given by Huang & Feng (1995). We are currently limited to two-dimensional simulations. Nonetheless, this is the first attempt, to our knowledge, at dynamic simulation of particle motion in complex flows of viscoelastic fluids.

2.1. Sedimentation of a single particle in a channel

The geometry of the problem is shown in figure 1. A cylinder of radius a and density ρ_s is released at an eccentric position in a channel filled with an Oldroyd-B fluid. The cylinder is heavier than the fluid and starts to settle under gravity. We wish to study the lateral motion of the particle as a result of the walls.

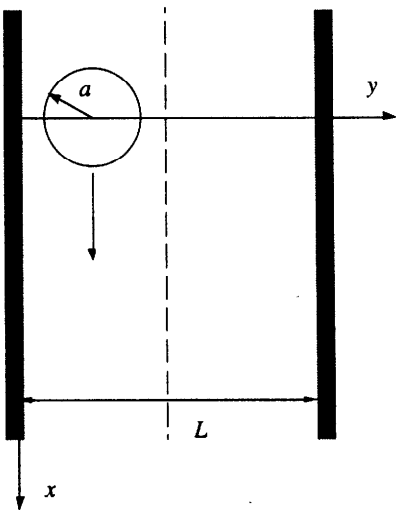

Figure 1. Sedimentation of a single cylinder in a channel filled with an Oldroyd-B fluid.

Before doing dynamic simulations of the sedimentation, we first carried out static calculations. The particle is fixed in space; a uniform velocity U is applied at the inlet of the domain and on both side walls. This is a Galilean transformation of a steady sedimentation without lateral migration and rotation. The lateral force on the particle then suggests the direction of lateral motion if the constraints are removed. Because dynamic simulations of sedimentation usually have long transients and require a tremendous amount of computation, we use static calculations to explore the effects of various parameters. Then a

complete picture of the sedimentation may be constructed by doing just a few dynamic simulations.

a. Static calculations

We use an Oldroyd-B model with $\lambda_2/\lambda_1=1/8$. The control parameters are $Re=\rho_f Ua/\mu$, $De=U\lambda_1/a$ and the blockage ratio L/a. We define a drag coefficient (C_d) and a lift coefficient (C_l) by dividing the forces by ($\rho_f U^2 a$), and a torque coefficient (C_t) by dividing the torque by ($2\rho_f U^2 a^2$).

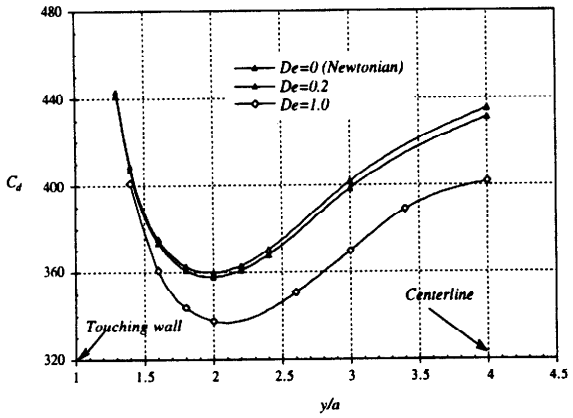

Figure 2. The drag on a cylinder at different positions. Re=0.05, L/a=8.

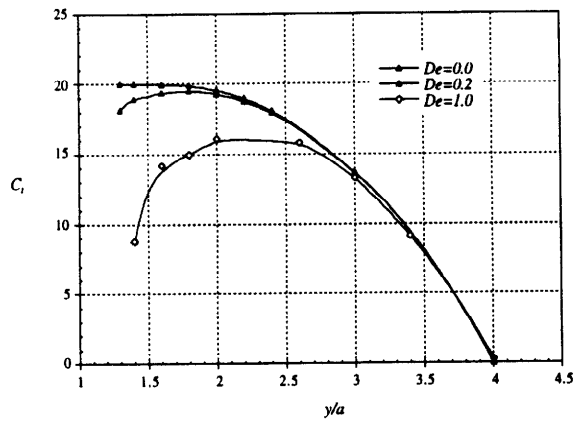

Figure 3. The torque on a cylinder at different positions. Re=0.05, L/a=8.

Results show that at relatively low Reynolds numbers, the drag has a minimum when the cylinder is somewhere between the centerline and the wall (figure 2). For L/a=8, this minimum occurs at $y/a \approx 2$. The minimum drag is consistent with the creeping flow results of Dvinsky & Popel (1987). As the Deborah number is increased, the drag is reduced. The torque on the cylinder is positive for $y<L/2$ (figure 3), meaning that the cylinder would rotate as if rolling up the nearby wall. Increasing De tends to reduce the magnitude of this torque.

The variation of the lateral force is much more intriguing. Typically, there is a region near the wall in which strong wall repulsion prevails. Between this *wall region* and the centerline of the channel is a *core region* in which the cylinder experiences attraction

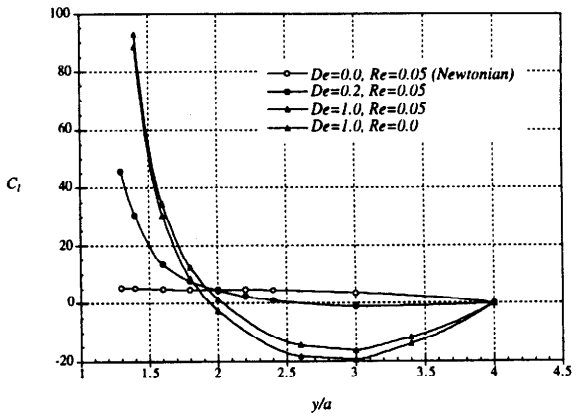

Figure 4. The lift on a cylinder at various lateral positions. L/a=8. The Deborah number tends to promote the attraction force while the Reynolds number tends to suppress it. A curve for Newtonian flow is also shown for comparison.

toward the nearby wall (figure 4). The effect of De is to promote wall attraction. At De=0, a wall repulsion prevails throughout the entire region, a well-known fact from previous study of Newtonian flows (Feng *et al.* 1994*a*). As De increases from 0.2 to 1, the core region becomes wider and the magnitude of the attraction force is greatly increased. The wall region is narrowed, though the repulsion force sees an increase. The effect of Re, on the other hand, is to suppress the wall attraction. As compared with the creeping flow (Re=0, De=1.0), the inertial flow at Re=0.05 and De=1.0 has a smaller core region with a weaker attraction force and a stronger repulsion in the wall region.

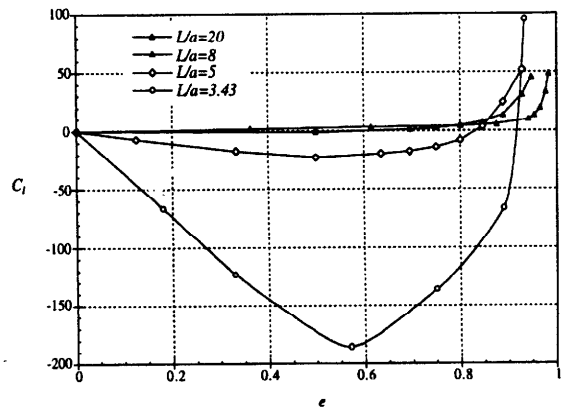

Figure 5. Effects of the blockage ratio L/a on the lift force. Re=0.05, De=0.2. The eccentricity factor e=0 on the centerline; e=1 when the cylinder touches one side wall.

The geometric parameter L/a has an unexpectedly strong effect on the lateral force. Narrower channels have a relatively wider core region with a larger attraction force (figure 5). To compare the lift curves in different channels, we use the eccentricity factor $e=1-d_1/d_2$, where d_1 and d_2 are the width of gaps on both sides of the particle. For L/a=3.43, the core region extends to e=0.92. On the other hand, no core region is observed for a wide channel of L/a=20; wall repulsion prevails throughout.

The above results imply that the wall attraction is not a result of a single wall, but rather is caused by two walls. This is different from the concept of wall attraction derived from experiments (Joseph *et al.* 1994, Jones *et al.* 1994). There are two possible explanations for this apparent discrepancy: (i) our numerical results are valid in two dimensions only, and the wall effects are markedly different in two and three dimensions; or (ii) the present results are qualitatively valid in three dimensions, and the previous notion of attraction toward a single wall is misguided. Wang *et al.* (1996) carried out a three-dimensional calculation in an enclosed domain. A perturbation scheme is used to extract the leading-order viscoelastic effects on the lateral force between a sphere and a nearby wall. A repulsion force is obtained in a region next to the wall and an attraction force exists further out. This result appears to be evidence for (ii). But it remains to be seen whether the core region will dwindle or even disappear when the other walls are moved away. Experimentally, Joseph *et al.* (1994) noticed that under certain conditions, a sphere does not come into contact with the wall but rather keeps a small stand-off distance. The effect of blockage shown in figure 5 also seems to be consistent with the falling-ball experiment of Tanner (1964).

b. Dynamic simulations

The transient sedimentation of particles with terminal velocity U_t depends on the Froude number $Fr=ga/U_t^2$ and the density ratio ρ_s/ρ_f besides Re, De and L/a. The dynamic behavior of a settling particle is manifest of the wall-particle interaction that we have learned from static calculations. The effect of the Deborah number is depicted in figure 6. The curves were obtained by varying the relaxation time of the fluid λ_1 while keeping other parameters fixed. Because the drag on the particle depends on De (Huang & Feng 1995), the terminal velocity U_t and thus Re and Fr also change. It is clear that larger De results in an equilibrium position closer to the channel wall, indicating a wider core region in which wall attraction prevails (cf. figure 4).

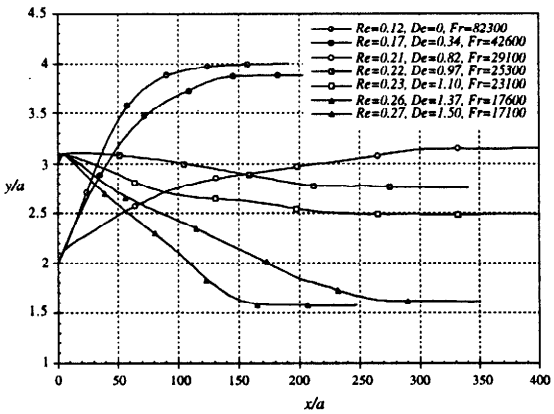

Figure 6. The effect of viscoelasticity on the trajectory of a particle settling in a channel. L/a=8, ρ_s/ρ_f=1.0007. Re, De and Fr all change as the relaxation time of the fluid λ_1 is changed.

2.2. Interaction of two particles settling in a channel

a. The vertical configuration

Riddle *et al.* (1977) observed in experiments that two spheres released tandem in a viscoelastic liquid will attract and come into touch if their initial separation is below a critical value that depends on the rheological properties of the fluid. If the initial separation exceeds this critical value, the two spheres will become farther apart during the settling.

We study the particle-particle interactions by static and dynamic simulations. In the static calculations, two circular particles of radius a are fixed on the centerline of a plane channel of width L=8a; the channel is filled with an Oldroyd-B fluid with λ_2/λ_1=1/8. The center-to-center distance between the particles is s. In this computation, the crucial factor is the drag forces on both particles. If the drag on the particle on top (D_1) is larger than that on the particle at the bottom (D_2), the two will separate during sedimentation. Contrarily, the particle on top will catch up with the bottom one if $D_2>D_1$. Figure 7 shows the variation of the drag coefficient at different separations. In the Newtonian case, the drag is essentially the same on the two particles. This is because the inertia is small at $Re=5\times10^{-3}$. At Deborah number De=1, particle 1 (on top) experiences a smaller drag than particle 2 if the particles are fairly close ($s/a<7$). In the range $7<s/a<9$, there is a reversal in the relative magnitude of the drag; the bottom particle has a slightly smaller drag. At s/a=10, the two drag forces are almost identical, indicating negligible interactions between particles at this separation or farther apart. Apparently, the static results are consistent with the experimental observations of Riddle *et al.* (1977).

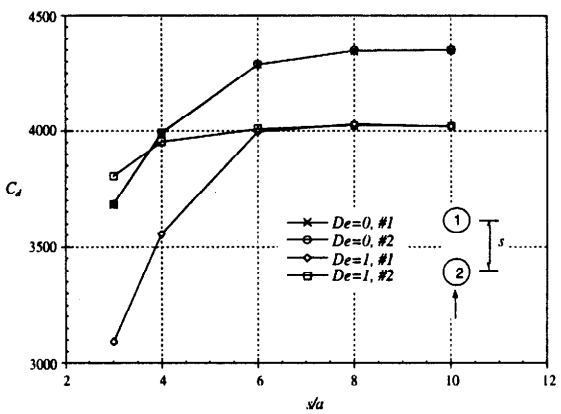

Figure 7. The drag forces on two particles fixed tandem in space. $Re=5\times10^{-3}$, L/a=8.

Dynamic simulations are done for inertialess flows (Re=0). This is in part because the behavior to be simulated has nothing to do with inertia, as is obvious from figure 7. This is also the case in the experiment of Riddle *et al.* (1977). An additional benefit is reduced computational cost; the nonlinear inertia requires a Newton iteration. The inertia of solid particles is retained.

Three dynamic runs are shown in figure 8. The particles are released at different initial separations: $s_0=4a$, $8a$ and $10a$. In the first case, the particle on top rapidly catches up with the other. When they become too close to each other, the simulation breaks down. In reality the particles will come into contact and fall as a doublet (Riddle *et al.* 1977). The other two runs are intended to demonstrate the weak repulsion force found in static calculations. This scenario turns out to be difficult to realize dynamically. For $s_0=8a$, the center-to-center distance s does tend to grow at the beginning. But this trend is quickly reversed, and the particles start to get closer slowly. For $s_0=10a$, s never increases; it maintains its initial value for a short time and then starts to decrease. Finally s seems to attain an equilibrium value at $9.85a$. The 'terminal' velocity is virtually the same in the last two cases; the doublet formed in the first case ($s_0=4a$) falls much faster.

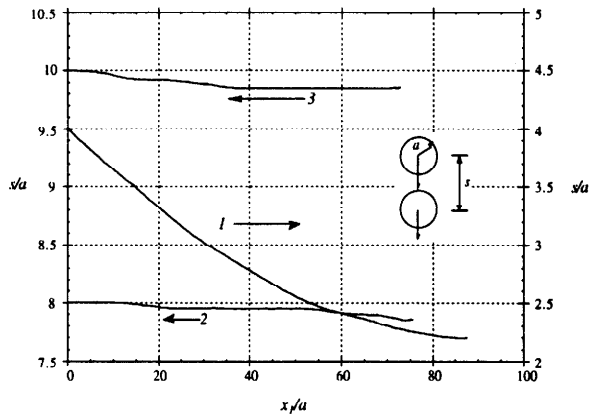

Figure 8. The interaction of two particles falling one on top of the other. The abscissa is the vertical distance traveled by the particle on top. L/a=8, ρ_s/ρ_f=1.0002, Re=0. (1) The initial center-to-center distance is s_0=4a. At the end of the simulation, De=0.3, Fr=2.18x10^5; (2) s_0=8a. At the end of the simulation, De=0.21, Fr=4.62x10^5; (3) s_0=10a. At the end of the simulation, De=0.21, Fr=4.62x10^5.

The failure to simulate the separation of particles is probably a result of the transient nature of the motion. During sedimentation, the velocities of the particles change constantly. This has two effects on the relative magnitude of the drag. Firstly, because of the unsteadiness, the drag forces will be different from those in a steady flow at the same velocity. Secondly, the Deborah number and Reynolds number based on the instantaneous velocity are different from the projected terminal values. Then the ranges of s/a corresponding to attraction and repulsion (cf. figure 7) may also be different. Therefore, the dynamic behavior of a pair of particles in sedimentation cannot be safely predicted from static forces based on their initial separation and the projected terminal velocity. Besides, the repulsion is very weak in our two-dimensional calculation and thus easily drown out in dynamic simulation. The situation seems to be different in three dimensions: the separation of spheres is a fairly robust feature in the experiment of Riddle *et al.* (1977).

b. The horizontal configuration

We will consider the interaction of two particles settling abreast. Joseph *et al.* (1994) reported that two spheres released side-by-side in a polymer solution attract and approach each other if their initial separation is not too large. This is in clear contrast to the inertial repulsion well documented for Newtonian flows (Jayaweera & Mason 1965). We again use static and dynamic simulations to study the particle-particle interaction in this configuration. The two particles are fixed or released symmetrically across the centerline of the channel with a center-to-center distance of s. The width of the channel is L=20a for static calculations.

The lateral force from static calculations is shown in figure 9. A positive lift on the left particle implies attraction. For a Newtonian fluid at Re=0.05, the two particles repel each other when they are close. This repulsion force diminishes when their separation increases and eventually gives way to an "attraction" force at s/a=10. This bogus attraction is actually a result of repulsion from side walls; in this configuration the particles are much closer to the nearby wall than they are from each other. If inertia is removed but normal stress introduced in the calculation (Re=0, De=1), the inter-particle force is reversed. A strong attraction force exists between the particles, and it decreases as the particles become farther apart. Eventually the attraction is replaced by a "repulsion", which is probably caused by wall attraction. When

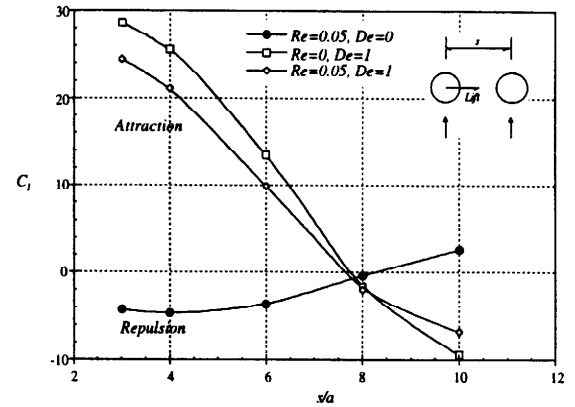

Figure 9. Inter-particle forces on a pair of particles fixed side by side in a channel. A Newtonian lift curve is also shown for comparison. L/a=20.

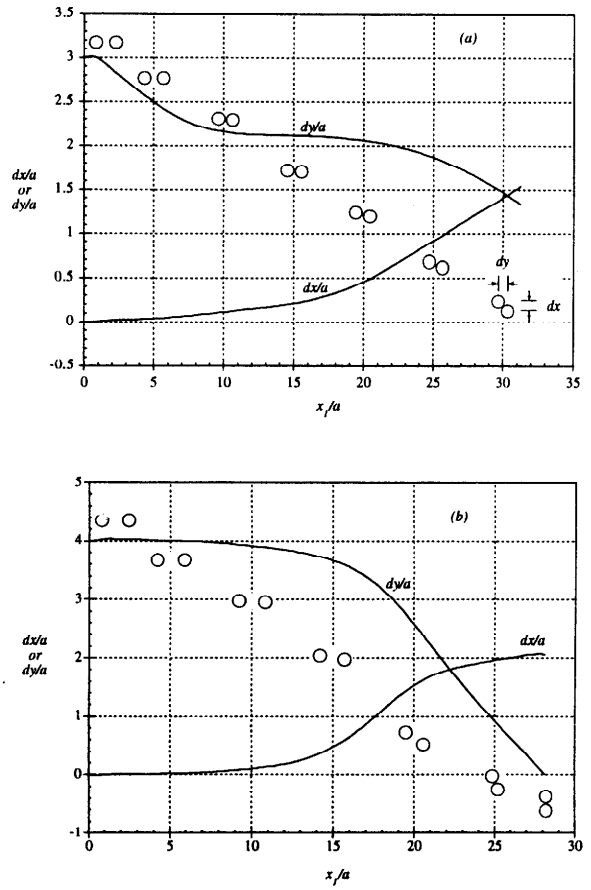

Figure 10. The interaction between a pair of particles released side by side. L/a=10, ρ_s/ρ_f=1.0005, Re=0. (*a*) Initial separation s_0=3a. At the end of the simulation De=1.8, Fr=1.36x10^4 for both particles. (*b*) Initial separation s_0=4a. At the end of the simulation De=1.43, Fr=2.17x10^4 for both particles.

inertia and normal stress coexist, as is the case in the experiments, the two mechanisms compete with each other and the outcome will depend on their relative strength. Figure 9 shows a lift curve at Re=0.05 and De=1; in this case the normal stress apparently has an upper hand.

For reasons given before, the fluid inertia is put to zero in dynamic simulations of two circular particles settling abreast. To reduce computational cost, we use a channel of L=10a, which is narrower than that used in the static computation. This is expected to have only qualitative effects on the behavior of the particles. Two simulations are shown in figure 10.

Immediately after the particles are dropped, they tend to repel each other and move apart. This initial transient is similar to that observed in figure 8. After that, the particles start to attract and approach each other, rotating in the mean time as if rolling up the vertical plane of symmetry between them. When the two particles are close enough, they behave like a single long particle, and as such begin to turn the line of centers toward the direction of settling. For this configuration, the inter-particle attraction in figure 7 kicks in. The two particles will eventually touch and fall as a long particle. The initial center-to-center distance has a subtle effect on the scenario. For smaller s_0 (figure 10a), the lateral approaching occurs first and the turning of the doublet follows. If $s_0$is relatively large (figure 10b), the turning and approaching happen simultaneously. When the doublet is slanted during the turning, it also drifts sideways as in a Newtonian fluid. At the end of both simulations, the doublet has come close to one side wall and wall effects start to interfere. Though the dynamic simulations in two-dimensions cannot be rigorously compared to the experiments (Joseph *et al.* 1994), they have correctly reproduced the qualitative features observed.

In summary, the interaction of two particles in sedimentation consists of two fundamental mechanisms: the attraction between neighboring particles and the preferred orientation of a long body. For a sedimenting spheroid, we have shown that viscoelastic normal stresses modify the pressure distribution on the particle (Feng *et al.* 1995), and a torque results that turns the long axis to vertical. The direct contribution of the normal stresses to the torque is relatively small. The attraction between neighboring particles can also be traced to a modified pressure distribution on them (Feng *et al.* 1996).

3. Experimental results and discussion

In this part of our study, we generate a torsional shear flow between parallel plates and record the motion and interaction of spheres and rods suspended in polymer solutions. Figure 11 is a sketch of the experimental setup. A and B are glass discs aligned to within 0.07 mm at the rim. A is driven by the motor E and B is fixed. The diameter of A is 22 cm. C is a cylindrical shroud that encloses the liquid. The gap between the edge of A and the inner surface of C is 0.5 cm. The gap H between A and B is measured to within 0.01 mm. D is a video or photo camera. After the shear is started, trajectories of single particles are recorded onto video tapes and later read by use of a VIA100 reticle unit. The maximum error in the radial position of the particle is 0.2 mm. The parallax error is estimated to be negligible. When suspensions of many particles are sheared, we use a photographic camera coupled with close-up lenses to capture the details of the particle interactions.

The viscoelastic liquids used are aqueous solutions of poly(ethylene oxide) (Polyox WSR301 from Union Carbide) of 0.5%, 1% and 2% concentrations. These solutions exhibit large normal stress differences and has a strong storage modulus (Joseph *et al.* 1994). We have used glycerin and Newtonian silicone fluids (Dow 200 fluids) in certain tests as a comparison with the polymer solutions. Polystyrene spheres with diameters ranging from 250 μm to 850 μm are used. The density of the material is 1.05 g/cm^3. Rod-like particles are cut from two kinds of plastic threads with density 1 g/cm^3 and 1.26 g/cm^3, respectively. The first density roughly matches that of polyox solutions and silicone oils while the second matches that of glycerin. The diameter of the rods ranges from 170 μm to 330 μm and the length from 0.5 to 4 mm.

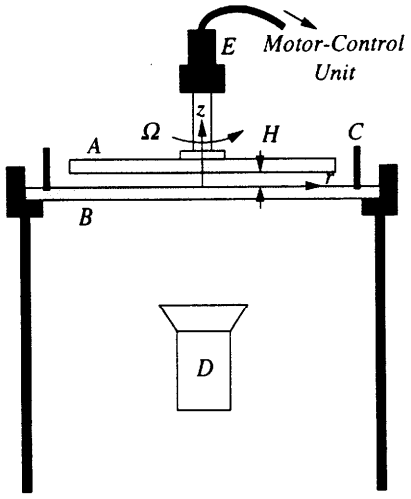

Figure 11. A sketch of the experimental setup.

All experiments are done in a temperature controlled room, and no further remedies are taken to counter viscous heating. We have repeatedly measured the temperature of the liquid before and after one hour of shearing at a typical shear-rate. The temperature rise is never over 1°C. Mechanical degradation is minor in our tests because the shear-rate is low (~ 20 s^{-1}) and the sample is used no longer than a week. It is well known that secondary recirculations occur in the parallel-plate type of apparatus. In our apparatus, the intensity of secondary flow is expected to depend on the gap size H and the angular velocity of the upper plate Ω. In preliminary tests, we have established the maximum values of H and Ω for each solution below which secondary recirculations can be safely neglected. All subsequent experiments were done within these limits.

3.1. Radial migration of a sphere

A sphere released in a 2% polyox solution migrates outward, and the radial velocity does not vary significantly with the radial position. Figure 12 shows a group of trajectories. Most part of each trajectory falls on a straight line, and its slope does not depend on r in a systematic way ($v_r \approx 4\times10^{-4}$ cm/s). Also shown is a trajectory of the same sphere in a 4,000 cst silicone oil. The viscosity of the oil matches that of the 2% polyox solution at the shear-rate that occurs near r=5 cm for the H and Ω values used. No radial migration is detected in two hours of shearing. This proves that the radial migration in the polyox solution is an effect of viscoelasticity. The longitudinal speed of the particle indicates its vertical position. Results show that the particle approaches the mid-plane between the plates independent of its initial location.

The results shown in figure 12 are quite different from the observations of Karis *et al.* (1984*b*) and Prieve *et al.* (1985). We obtained only outward migrations, and the radial velocity does not

depend on the radial position r. Prieve *et al.* (1985) observed inward and outward migrations separated by a critical streamline, and the absolute value of the radial velocity increases linearly with r inside and outside the critical radius. The liquid used here is shear-thinning and that used by Prieve *et al.* has a nearly constant viscosity in the range of shear-rate covered; shear-thinning may play a role in the dependence of v_r on r. Choi *et al.* (1987) suggested that the critical shear-rate is related to the relaxation time of the fluid such that the critical radius would be larger for more dilute solutions. In our device the smallest radius observable on the plate is r=3 cm, inside which the shaft prevents visual observation. It is possible that our 2% solution is too concentrated for the inward migration to be recorded. From this consideration we repeated the tests in figure 12 with 1% and 0.5% polyox solutions.

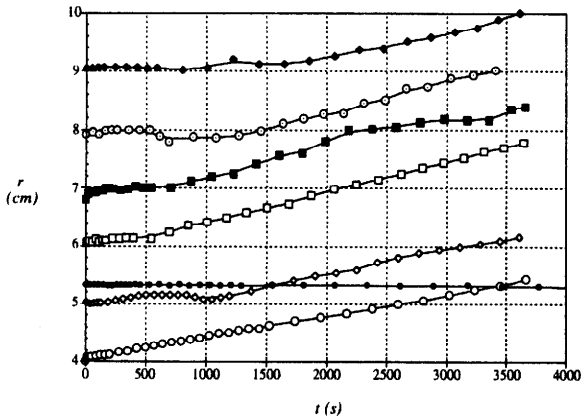

Figure 12. Radial migration of spheres in 2% polyox solution. The diameter of the sphere d=580 μm. H=2 mm, Ω=2.55 rpm. Also shown is the radial motion of the same sphere in a silicone oil (filled circles).

Because of the reduced viscosity of the more dilute solutions, lower angular velocity Ω has to be used lest secondary recirculation develops between the plates. On the other hand, if Ω gets too small, the radial migration becomes very weak and hard to measure. For the 1% solution, we have observed only outward migration. The velocity of migration, if scaled by ΩR (R is the radius of the upper disc), is about one half of that in the 2% solution for a sphere of the same size. Results obtained in the 0.5% solution are less repeatable than in the other two solutions. Qualitatively speaking, slow inward migration occurs at all radial positions with a radial velocity on the order of 5×10^{-5} cm/s. This seems to agree with the arguments of Choi *et al.* (1987). We cannot confirm the existence of critical streamlines and the discontinuous migration velocity reported by Karis *et al.* (1984*b*).

3.2. Rotation and migration of rod-like particles

We have found two modes of motion for a rod in 2% polyox solution, depending on the local shear-rate, the initial configuration and the rod's aspect ratio. The first mode occurs only if the shear-rate is low and the rod is initially oriented close to the radial direction. Then the rod executes an oscillating motion along a Jeffery orbit around the local vorticity vector. Previous experiments in Couette flows (Gauthier *et al.* 1971*a*) suggested that viscoelasticity would drive the rod into a preferred Jeffery orbit with its axis completely aligned with the vorticity vector (orbit constant C=0). In our experiment, the rod is initially assigned an orbit close to the preferred one. In the time of observation (typically 10 minutes), the rod seems to maintain the same orbit and no evolution is detected. Perhaps, inertia has prevented complete evolution and forced an equilibrium orbit close to C=0. The period of rotation is in general much longer than the theoretical value for the Jeffery orbit. The discrepancy seems to be larger at higher shear-rates.

If the same rod is initially oriented such that it makes a relatively large angle with the local vorticity, or if the shear-rate is high enough, the rod immediately aligns itself with the local streamline upon start of the flow. Then it will stay aligned and be carried along by the flow. This is the second mode of motion, or 'aligned motion'. Rods with larger aspect ratios align with the flow more easily. For instance, a thin rod with L=1.8 mm and r_p=10.6 aligns immediately with the flow at the smallest shear-rate tested in our device (~1.8 s^{-1}), even if it is carefully oriented in the radial direction before the shear starts.

The same two modes of motion have been observed in 1% polyox solution; all qualitative features of the motion are the same. The oscillating motion, however, persists up to higher shear-rates than in the 2% solution; the oscillation also achieves larger amplitude. Besides, the period of rotation is shorter and closer to the theoretical value for Newtonian fluids. These differences are consistent with the fact that rheologically the 1% solution is between a Newtonian fluid and the 2% solution.

To summarize, the oscillating motion prevails only if the shear-rate and initial orientation fall into a small window. This window is affected by the aspect ratio of the rod and the properties of the fluid. Larger aspect ratio and larger normal stresses tend to shrink the window, though it is not clear whether it can be completely eliminated. The behavior of a rod in a torsional flow appears to be qualitatively the same as in a Couette flow (Karnis & Mason 1966, Gauthier *et al.* 1971*a*, Bartram *et al.* 1975). The perturbation analyses of Leal (1975) and Brunn (1980) showed that the second normal stress difference causes an orbit drift toward C=0. When the shear-rate is sufficiently large, a steady solution emerges with the rod aligned with the flow. The rod selects one of the two solutions based on its initial orientation. This picture is entirely consistent with our findings.

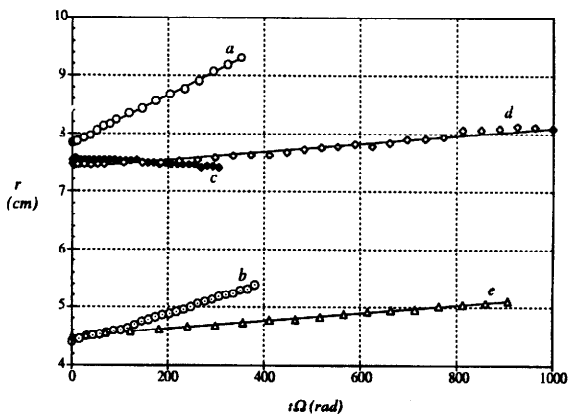

Figure 13. Radial migration of neutrally buoyant rods in polyox solutions. H=2 mm. (*a*) The length and diameter of the rod are L=1 mm and d=330 μm. Ω=3.9 rpm. Aligned motion in 2% solution with radial velocity $v_r=1.67\times10^{-3}$ cm/s. (*b*) Same as 1 except for a different initial position; $v_r=1.03\times10^{-3}$ cm/s. (*c*) Same as 1 except that the rod is in oscillating motion. Ω=1.6 rpm, $v_r=-7.71\times10^{-5}$ cm/s, $C\approx0.1$. (*d*) Same as 1 but the rod is longer L=1.8 mm; $v_r=2.81\times10^{-4}$ cm/s. (*e*) Same as 2 but in 1% polyox solution; $v_r=2.82\times10^{-4}$ cm/s.

Radial migration is observed for rods in viscoelastic fluids, being inward if they are in the oscillating mode of motion and outward if the aligned mode prevails. In both cases, rods migrate at a constant radial velocity v_r (figure 13). For outward migration (curve *a*), the non-dimensional radial velocity $v_r/\Omega R$ is about 8 times larger than that for inward migration (curve *c*). The outward migration is slower for a longer rod (curve *d*). This is somewhat surprising since a rod seems to migrate much faster than a sphere of the same diameter (cf. figure 12 and curve 1 in figure 13). In 1% polyox solution, v_r is about 1/4 of that in the 2% solution, other conditions being the same (curve *e*). In both modes of motion, the angular velocity with which the rod revolves around the hub approaches $\Omega/2$, indicating that the rod drifts vertically to the midplane between the plates.

3.3. Behavior of suspension of spheres

Polystyrene spheres are added to 2%, 1% and 0.5% aqueous polyox to form suspensions. The diameter of the spheres ranges from 250 μm to 850 μm; we used the particles directly out of the bottle and the size distribution is unknown. The solid volume fractions used are 2%, 5% and 10%.

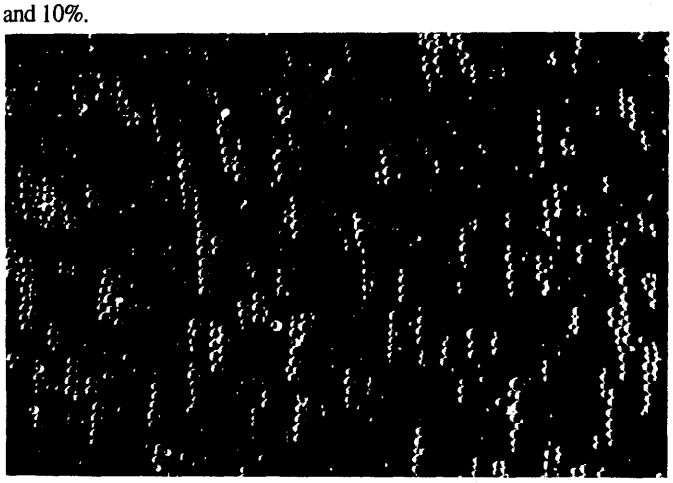

(*a*)

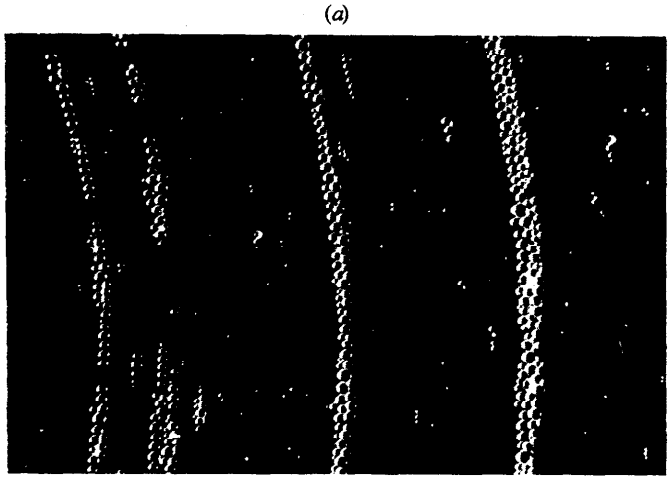

(*b*)

Figure 14. Formation of microstructures in 2% suspension of spheres in 2% aqueous polyox. H=2.1 mm. (*a*) after 2 minutes of shearing at Ω=3.5 rpm; (*b*) after 18 minutes of shearing.

Once the flow starts, spheres interact with one another and microstructures form. The characteristics of this process are the same for suspensions of various solid fractions in different solutions. Figure 14 shows snapshots of a 2% suspension in 2% aqueous polyox. The flow direction is from bottom to top in the photographs.

Shortly after the shear starts, spheres near the outer edge, where the shear is the strongest, start to form short chains that are aligned to the flow. Such chains appear throughout the suspension after 2 minutes of shearing (frame *a*). In this picture, the chains comprise mostly of larger spheres. After 8 minutes of shearing, the chains have connected to form longer strings. Neighboring chains apparently attract each other and they aggregate to make the string thicker. It may also be noticed that smaller spheres start to form their own chains. This size selection in particle-particle interaction agrees with previous observations of Giesekus (1981). After 12 minutes of shearing, the strings have further grown in length and thickness, and become complete circular rings. These rings continue to absorb short chains until only a few spheres are left in the clear liquid between adjacent rings (frame *b*).

The rings migrate outward; the interior of the flow field will be depleted of all solids in a certain time. One might expect spheres of different size to migrate at different speed, therefore causing disintegration and regrouping of rings. This does not happen. Most rings survive the migration and reach the rim as a whole. Occasionally, a thin ring breaks up as its diameter grows. Then all spheres will be absorbed by the next ring; no dispersion of spheres is observed. When rings first appear, they are more or less evenly spaced. After the first few rings on the outside have arrived at the rim, the ring spacing on the inside grows. After the solid concentration has dropped considerably near the hub, thinner rings emerge. They are also closer to one another. The rings rotate at roughly half the speed of the upper plate, suggesting that they prefer a vertical position midway between the plates.

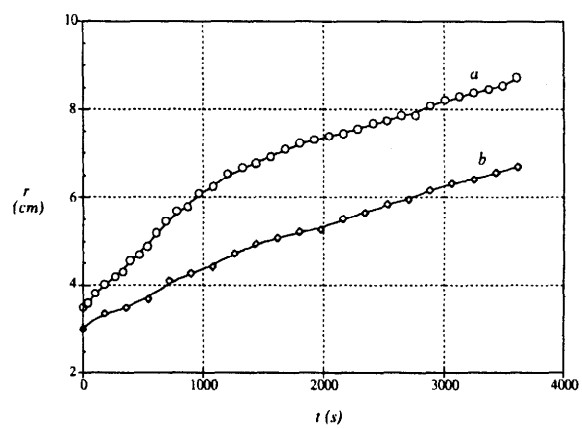

Figure 15. The outward migration of rings in 10% suspension of spheres in 2% aqueous polyox. H=2.1 mm, Ω=3.5 rpm. Ring *a* is a thick ring that appears in an early stage and *b* is one of the thin rings that appear later; the time has been shifted for comparison.

The radial migration of rings is measured in one case using 10% solids in 2% aqueous polyox. Figure 15 shows the migration of two rings: *a* is a thick ring that appears in an early stage and *b* is one of the thin rings that appear later. Ring *a* starts with a high speed and then settles into a slower speed v_r=8.68x10^{-4} cm/s. The same pattern holds

for ring b. Though its initial migration is slower, ring b later attains essentially the same velocity as a (v_r=8.40x10^{-4} cm/s). Another intriguing feature of the migration is that rings, comprised of spheres of various sizes, migrate much faster than a single sphere under the same shear (cf. figure 12).

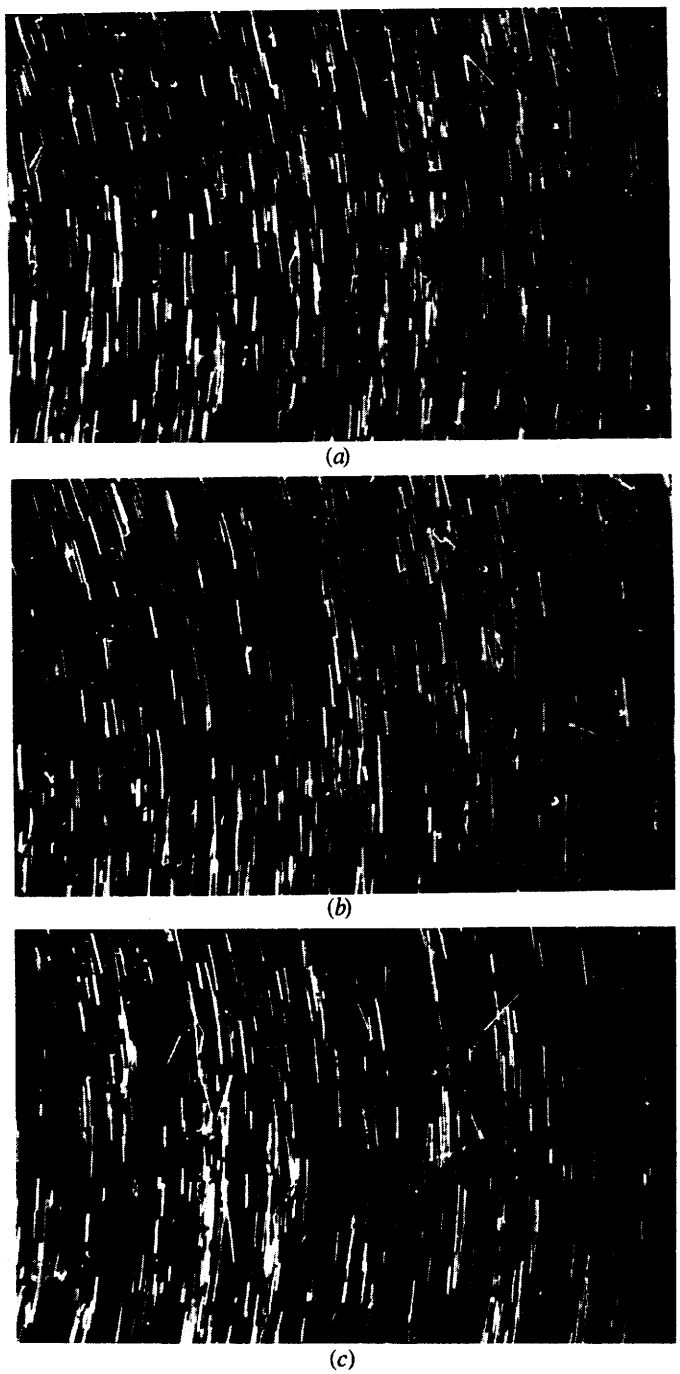

Figure 16. The formation of microstructures in 2% suspension of rods in 1% aqueous polyox. H=2.6 mm. (a) after 7.7 minutes of shearing at Ω=5.75 rpm; (b) after 9 minutes of shearing at Ω=12.1 rpm following the last frame; (c) after 30 seconds of shearing at Ω=31.1 rpm following the last frame.

3.4. Behavior of suspension of rods

Plastic rods of diameter d=170 ~ 330 μm and length L=0.5 ~ 4 mm are mixed with 1% polyox solutions. The mixture is stirred thoroughly and sits still for a few hours to let the air bubbles out before being loaded on our parallel-plate device. Two suspensions of 2% and 5% solid volume fractions are studied and the behavior is similar. Figure 16 shows a sequence of snapshots of the suspension.

After the flow starts, most rods align themselves with the flow direction in a few seconds. After 7 minutes of shearing at Ω=5.75 rpm (frame a), some rods seem to have formed chains. But this is much less obvious than with the spheres (cf. figure 14a). Also unlike suspensions of spheres, the suspension of rods is still more or less homogeneous; no large aggregates of particles are found. Then the angular velocity of the upper plate is suddenly raised to Ω=12.1 rpm. At this high shear-rate, rod chaining, aggregation and outward migration are all accelerated. After 9 minutes' shearing (frame b), more chains have formed and the suspension becomes nonhomogeneous with aggregates of rods and areas of clear liquid. At this point, Ω is increased to 31.1 rpm. After 30 seconds of shearing (frame c), band-like structures can be discerned. As compared with the rings of figure 14, these structures of assembled rods are much less conspicuous; many thin chains and single rods fill the space between the aggregates. The rods migrate outwards in the radial direction.

We may conclude from figure 16 that rod-like particles align with the flow. They also associate with one another to form chains and aggregates. These interactions are much weaker than those among spherical particles.

3.5. Discussion on microstructures

Two major results of this experimental study are the migration of particles in a torsional flow and interaction and aggregation among particles. Obviously, complete interpretations of these phenomena are not yet available. Here we will briefly discuss the local hydrodynamic mechanisms that lead to the formation of chain-like aggregates aligned with the flow.

Petit & Noetinger (1988) offered an explanation for the chains in terms of the secondary flow induced by the spheres' rotation. Since a rotating sphere in a viscoelastic fluid sucks in fluid around its equator and ejects fluid from its two poles, two spheres whose line of center is parallel to the streamlines in a shear flow will attract each other. More spheres join in to form a chain. This theory is unlikely to be true for three reasons. Firstly, it has been observed that once the spheres form a chain, they stop rotating (Michele *et al.* 1977). Hence rotation-induced suction cannot be the agent to hold the chain together. Secondly, the secondary flow implies repulsion between spheres rotating side by side. This cannot explain the rings made of several chains bundled together (figure 14). Finally, rod-like particles do not rotate but they do form chains and aggregates.

Since all interactions happen on the plane of uniform velocity, the effect of shear is minimal. We believe the mechanisms for particle-particle interaction and association are the same ones that operate in the sedimentation and fluidization of many particles in a viscoelastic liquid. The two basic mechanisms found in sedimentation are:

(i) Attraction force between particles falling side by side (Joseph *et al.* 1994) or one on top of the other (Riddle *et al.* 1977).

(ii) Preferred orientation of a long particle in sedimentation with its long axis parallel to the direction of fall (Leal 1975, Liu & Joseph 1993).

Numerical simulations have revealed the anatomy of these mechanisms (Feng *et al.* 1995, 1996). Viscoelastic normal stresses cause a dramatic change in the pressure distribution near the particle.

This new pressure field yields forces and torque that are opposite to those expected in a Newtonian fluid; the direct contribution of the normal stresses to the forces is relatively small. We should also mention that when the separation between two spheres falling one on top of the other exceeds a threshold value ($5d$~$10d$), a weak repulsion exists between them (Riddle *et al.* 1977). This should not affect the picture of particle aggregation in an important way.

Thus, if a suspension in viscoelastic liquids is sheared, particles attract each other in longitudinal and lateral directions. Primitive arrays made of spheres joined abreast will rotate until they too are aligned with the flow. Parallel chains attract each other and form thicker aggregates. Inhomogeneity develops just like in sedimentation (Allen & Uhlherr 1989, Joseph *et al.* 1994). Since thin rods aligned with the stream cause little disturbance to the ambient flow, the range of the lateral attraction force is much shorter for rods. Hence, fiber-like particles aggregate much more slowly (figure 16).

4. Conclusions

This paper investigates the viscoelastic effects on the motion and interaction of particles in sedimentation and torsional shear flow. The main results of this paper may be summarized as follows.

(1) For a particle settling in a vertical channel, viscoelasticity generates a wall repulsion if the particle is very close to the wall and a wall attraction if they are farther apart. The particle will approach an eccentric equilibrium position which depends on the Reynolds and Deborah numbers.

(2) Two particles settling one on top of the other attract and approach each other if their initial separation is not too large.

(3) Two particles settling side by side attract and approach each other. The doublet rotates till the line of centers is aligned with the direction of fall.

(4) In a torsional flow of viscoelastic liquids, spherical and rod-like particles migrate radially under the action of normal stresses. The direction of migration depends on the properties of the fluid and the motion of the particle. The velocity of migration does not depend strongly on the radial position.

(5) The rotation of a rod-like particle in a torsional flow is essentially the same as in a simple shear flow.

(6) Suspensions of spheres and rods in viscoelastic liquids exhibit microstructures under shear. Chains and aggregates of particles form and are aligned with the flow direction. Microstructures and inhomogeneity develop more readily for spheres than for rod-like particles.

(7) The mechanisms for particle interaction and aggregation in shear flows are believed to be the same ones found in sedimentation: attraction forces among particles and preferred orientation of long particles.

Acknowledgment: This work was supported by the NSF Grand Challenge HPCC grant (ECS 9527123), the US Army, Mathematics and AHPCRC, the DOE, Department of Basic Energy Sciences, the Schlumberger Foundation and the Minnesota Supercomputer Institute. J.F. acknowledges support from the Graduate School of the University of Minnesota through a Doctoral Dissertation Fellowship.

References

Advani, S. & Tucker, C. L. 1987 The use of tensors to describe and predict fiber orientation in short fiber composites. *J. Rheol.* **31**, 751-784.

Ait-Kadi, A. & Grmela, M. 1994 Modelling the rheological behavior of fiber suspensions in viscoelastic media. *J. Non-Newtonian Fluid Mech.* **53**, 65-81.

Allen, E. & Uhlherr, P. H. T. 1989 Nonhomogeneous sedimentation in viscoelastic fluids. *J. Rheol.* **33**, 627-638.

Bartram, E., Goldsmith, H. L. & Mason, S. G. 1975 Particle motion in non-Newtonian media III. Further observations in elasticoviscous fluids. *Rheol. Acta* **14**, 776-782.

Brunn, P. 1977 Interaction of spheres in a viscoelastic fluid. *Rheol. Acta* **16**, 461-475.

Brunn, P. 1980 The motion of rigid particles in viscoelastic fluids. *J. Non-Newtonian Fluid Mech.* **7**, 271-288.

Caswell, B. 1972 The stability of particle motion near a wall in Newtonian and non-Newtonian fluids. *Chem. Eng. Sci.* **27**, 373-389.

Chan, P. C.-H. & Leal, L. G. 1977 A note on the motion of a spherical particle in a general quadratic flow of a second-order fluid. *J. Fluid Mech.* **82**, 549-559.

Choi, H. J., Prieve, D. C. & Jhon, M. S. 1987 Anomalous lateral migration of a rigid sphere in torsional flow of a viscoelastic fluid - effect of polymer concentration and solvent viscosity. *J. Rheol.* **31**, 317-321.

Dinh, S. M. & Armstrong, R. C. 1984 A rheological equation of state for semiconcentrated fiber suspensions. *J. Rheol.* **28**, 207-227.

Dvinsky, A. S. & Popel, A. S. 1987 Motion of a rigid cylinder between parallel plates in Stokes flow. Part 1. Motion in a quiescent fluid and sedimentation. *Computers & Fluids* **15**, 391-404.

Feng, J., Hu, H. H. & Joseph, D. D. 1994*a* Direct simulation of initial value problems for the motion of solid bodies in a Newtonian fluid. Part. 1. Sedimentation. *J. Fluid Mech.* **261**, 95-134.

Feng, J., Hu, H. H. & Joseph, D. D. 1994*b* Direct simulation of initial value problems for the motion of solid bodies in a Newtonian fluid. Part. 2. Couette and Poiseuille flows. *J. Fluid Mech.* **277**, 271-301.

Feng, J., Huang, P. Y. & Joseph, D. D. 1996 Dynamic simulations of sedimentation of solid particles in an Oldroyd fluid. *J. Non-Newtonian Fluid Mech.* **63**, 63-88.

Feng, J., Joseph, D. D., Glowinski, R. & Pan, T. W. 1995 A three-dimensional computation of the force and torque on an ellipsoid settling slowly through a viscoelastic fluid. *J. Fluid Mech.* **283**, 1-16.

Gauthier, F., Goldsmith, H. L. & Mason, S. G. 1971*a* Particle motions in non-Newtonian media I. Couette flow. *Rheol. Acta* **10**, 344-364.

Gauthier, F., Goldsmith, H. L. & Mason, S. G. 1971*b* Particle motions in non-Newtonian media II. Poiseuille flow. *Trans. Soc. Rheol.* **15**, 297-330.

Giesekus, H. 1981 Some new results in suspension rheology. in *Non-Newtonian Flows*, Lecture Series 1981-6, ed. J. F. Wendt, von Karman Institute for Fluid Dynamics.

Highgate, D. J. & Whorlow, R. W. 1968 Migration of particles in a polymer solution during cone and plate viscometry. in *Polymer Systems: Deformation and Flow*, edited by R. E. Wetton & R. W. Whorlow, MacMillan, 251-261.

Ho, B. P. & Leal, L. G. 1976 Migration of rigid spheres in a two-dimensional unidirectional shear flow of a second-order fluid. *J. Fluid Mech.* **76**, 783-799.

Huang, P. Y. & Feng, J. 1995 Wall effects on the flow of viscoelastic fluids around a circular cylinder. *J. Non-Newtonian Fluid Mech.* **60**, 179-198.

Jayaweera, K. O. L. F. & Mason, B. J. 1965 The behavior of freely falling cylinders and cones in a viscous fluid. *J. Fluid Mech.* **22**, 709-720.

Jones, W. M., Price, A. H. & Walters, K. 1994 The motion of a sphere falling under gravity in a constant-viscosity elastic liquid. *J. Non-Newt. Fluid Mech.* **53**, 175-196.

Joseph, D. D., Liu, Y. J., Poletto, M. & Feng, J. 1994 Aggregation and dispersion of spheres falling in viscoelastic liquids. *J. Non-Newtonian Fluid Mech.* **54**, 45-86.

Karis, T. E., Prieve, D. C. & Rosen, S. L. 1984*a* Lateral migration of a rigid sphere in torsional flow of a viscoelastic fluid. *AIChE J.* **30**, 631-636.

Karis, T. E., Prieve, D. C. & Rosen, S. L. 1984*b* Anomalous lateral migration of a rigid sphere in torsional flow of a viscoelastic fluid. *J. Rheol.* **28**, 381-392.

Karnis, A. & Mason, S. G. 1966 Particle motions in sheared suspensions. XIX. Viscoelastic media. *Trans. Soc. Rheol.* **10**, 571-592.

Leal, L. G. 1975 The slow motion of slender rod-like particles in a second-order fluid. *J. Fluid Mech.* **69**, 305-337.

Leal, L. G. 1979 The motion of small particles in non-Newtonian fluids. *J. Non-Newtonian Fluid Mech.* **5**, 33-78.

Leal, L. G. 1980 Particle motion in a viscous fluid. *Ann. Rev. Fluid Mech.* **12**, 435-476.

Liu, Y. J. & Joseph, D. D. 1993 Sedimentation of particles in polymer solutions. *J. Fluid Mech.* **255**, 565-595.

Liu, Y. J., Nelson, J., Feng, J. & Joseph, D. D. 1993 Anomalous rolling of spheres down an inclined plane. *J. Non-Newtonian Fluid Mech.* **50**, 305-329.

Michele, J., Patzold, R. & Donis, R. 1977 Alignment and aggregation effects in suspensions of spheres in non-Newtonian media. *Rheol. Acta* **16**, 317-321.

Petit, L. & Noetinger, B. 1988 Shear-induced structures in macroscopic dispersions. *Rheol. Acta* **27**, 437-441.

Prieve, D. C., Jhon, M. S. & Koenig, T. L. 1985 Anomalous lateral migration of a rigid sphere in torsional flow of a viscoelastic fluid. II. Effect of shear rate. *J. Rheol.* **29**, 639-654.

Riddle, M. J. , Narvaez, C. & Bird, R. B. 1977 Interactions between two spheres falling along their line of centers in a viscoelastic fluid. *J. Non-Newtonian Fluid Mech.* **2**, 23-35.

Tanner, R. I. 1964 Observations on the use of Oldroyd-type equations of state for viscoelastic liquids. *Chem. Eng. Sci.* **19**, 349-355.

Toll, S. & Andersson, P. O. 1993 Microstructure of long- and short-fiber reinforced injection molded polyamide. *Polym. Compos.* **14**, 116-125.

Wang, W. Y., Feng, J. & Joseph, D. D. 1996 A numerical study of sphere-wall and sphere-sphere interactions in slow flow of non-Newtonian fluids. (in preparation).

AMD-Vol. 217

RHEOLOGY AND FLUID MECHANICS OF NONLINEAR MATERIALS — 1996 —

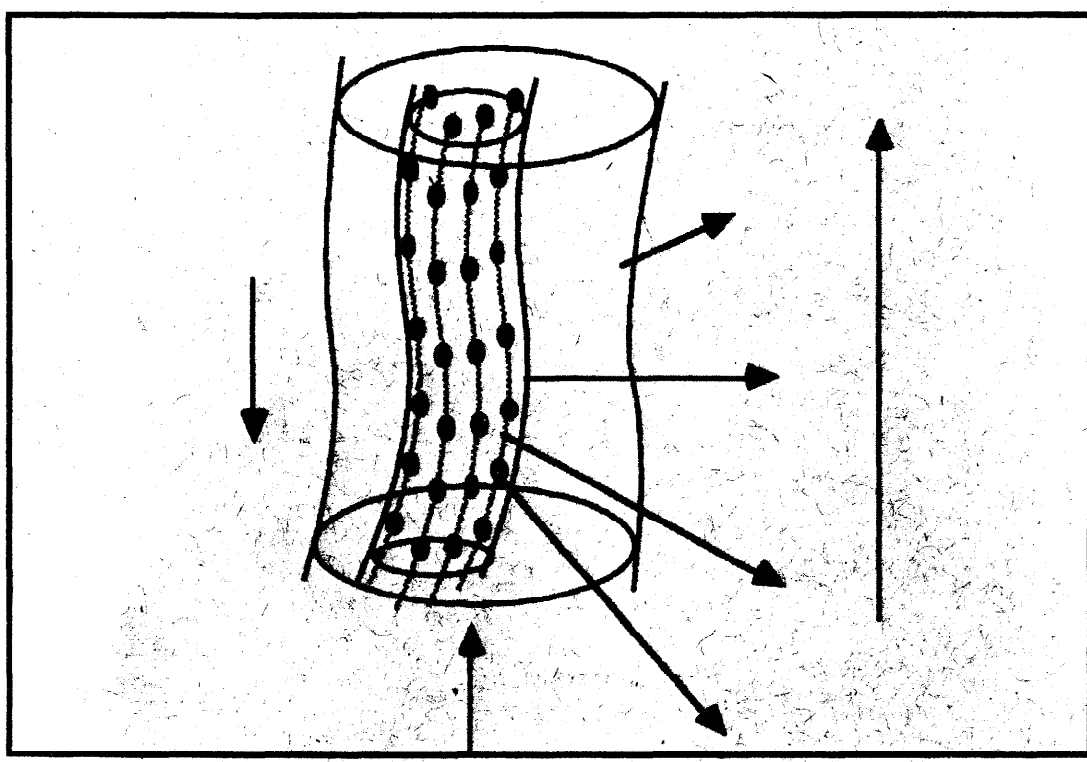

EDITED BY
D. A. SIGINER
S. G. ADVANI

1996 ASME INTERNATIONAL MECHANICAL ENGINEERING CONGRESS AND EXPOSITION